Journal of Materials Chemistry C

Accepted Manuscript

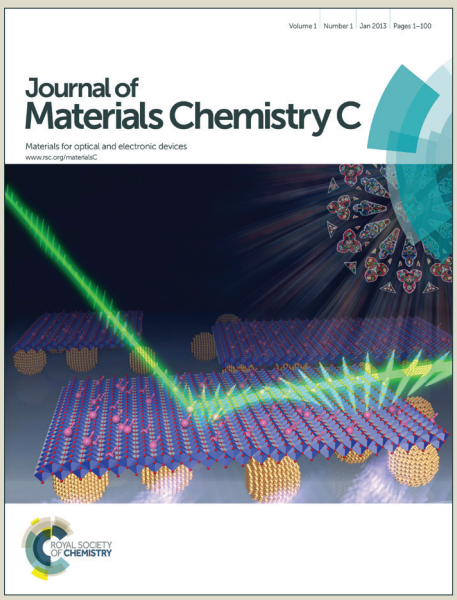

ROYAL SOCIETY OF CHEMISTRY

www.rsc.org/materialsC

Glycol modified Gadolinium oxide nanoparticles as potential template for selective and sensitive detection of 4-nitrophenol

Savita Chaudhary*, Sandeep Kumar, S.K. Mehta

Department of Chemistry and Centre of Advanced Studies in Chemistry, Panjab University, Chandigarh 160014, India

*Corresponding author
E-mail address: schaudhary@pu.ac.in
Tel: +91 9417250377; Fax: +91 172 2545074

Abstract

The highly efficient and simplistic fluorescence sensing method for estimating p-Nitro phenol (PNP) using surface functionalized Gd_2O_3 nanoparticles was developed. The surface morphology, structural characterization of Gd_2O_3 nanoparticles were analytically done by TEM, SEM, EDX, PXRD, TGA, FTIR, UV and fluorescence studies. All the surface functionalized particles have shown an evident green emitted light under UV lamp. The corresponding strong molecular interactions between the surface functionalized Gd_2O_3 nanoparticles and PNP resulted in the significant quenching of Gd_2O_3 nanoparticles as function of concentration and nature of nitro compounds with higher selectivity and sensitivity. The obtained limit of detection ranges from 3.9×10^{-7} M to 7.1×10^{-7} M. The reproducibility of results were also examined for all the under studied systems and was found that prepared samples were quite stable with relative standard deviation of 1.1% for Eg, 1.25% DEG, 1.6% TEG and 1.4% TeEG respectively. The influence of the surface capping over Gd_2O_3 nanoparticles for PNP sensing was further investigated for real samples with relative standard deviations below 3.2%. The outcomes endowed with an effectual mean to develop a sensor for fast detection and determination of perilous aromatic nitro compounds.

Keywords: Gd_2O_3 nanoparticles; Fluorescence sensing; p-Nitro phenol; Selectivity; Sensitivity

1. Introduction

Aromatic nitro compounds (ANCs) are unique category of chemicals utilized in different areas comprising pharmaceuticals, dyes, leather processing and pesticides industries.[1,2] ANCs are one of the important components for preparing explosives. These compounds also possess high stability, bioaccumulation ability with minimum tendency towards degradation in nature and have also been considered as a category of toxic organic contaminants.[3-5] The quantitative release of these toxin effluents into water bodies and surrounding environment create a massive risk to nature, inducing multiple human health disorders including carcinoma, anaemia and liver damage.[6, 7] Thus, from the perspective of human wellbeing and ecological safety, the sensing of ANCs have deserves special considerations of scientist. Till date, there are number of techniques such as high-performance liquid and gas chromatography (GC), electrochemical sensing and mass spectrometric analysis are utilized for the determination of ANCs.[8-11] However, all these techniques are time-consuming, unreasonably expensive and often required pre-treatments of the sample. For that reason, developing the highly selective and sensitive methods for ultra low sensing of ANCs by efficient and inexpensive method remains a progressive area of investigation. Consequently, we have carried out efforts to conquer these shortcomings by examining the fluorescence quenching of luminescent rare earth oxide materials.

The profiling of multifunctional luminescent rare earth oxide materials at nanometric range has unlocked the new horizons of developments in material science and nanomedicine.[12,13] The magnetic and fluorescent properties of lanthanide oxide based nanoparticles make them useful in diagnostic, imaging, and therapeutic applications.[14-16] The large stokes shift, sharp emission peaks, elongated life span, variations of excitation wavelength and decreased photobleching makes lanthanide oxide nanoparticles as efficient fluorescent label materials.[17,18] The optical properties generated in lanthanide oxide nanoparticles due to the presence of 4f electrons make them potential contender in the area of optical transmission, biomedical probes, fiber-optic amplifiers, lasers, waveguides and luminescent devices.[19-21]

Amongst a wide range of lanthanide oxide based nanoparticles, the potential applications of Gadolinium oxide (Gd_2O_3) nanoparticles are phenomenally multilateral.[22] Gd_2O_3 nanoparticles are particularly of high concern owing to their single phase multi-efficient bio-probe that provides combined magnetic, optical and luminescent activities in one particle.[23-25] Gd_2O_3 nanoparticles are one of the significant host materials for up-conversion

fluorescence.[26] Gd_2O_3 nanoparticles have unique applications in MRI contrast agent due to its large magnetic moments (seven unpaired electrons). The higher relaxation rate and quick renal excretion also enhances the popularity of Gd_2O_3 nanoparticles in comparison to other Gd based chelates.[27] Therefore, the simplistic means to assemble the constituents of the next generation technologies in fluorescence sensing with controlled morphology and surface electronic states represent an important confront in the field of nanoscaled sciences.

In the present work, the synthesis of Gd_2O_3 nanoparticles has been carried out by coordinating the surface of nanoparticles with ethylene (EG), diethylene (DEG), triethylene (TEG) and tetraethylene glycol (TeEG). Glycols have been chosen in order to discriminate between their surfaces capping ability over nanoparticles with respect to the chain length of alkyl groups. We also anticipate that the presence of glycols would decrease the size of the nanoparticles, as the availability of hydroxyl group possesses higher affinity to attach over the surface of nanoparticles. As compared to the bare Gd_2O_3 nanoparticles, the surface functionalized Gd_2O_3 nanoparticles have possesses lower value of non-radiative energy losses due to the presence of effective coating over the exterior surface of nanoparticles. Moreover, the surface capping of glycols over Gd_2O_3 nanoparticles effect the band gap of lanthanide oxides particles which further contributes towards the fluorescence properties of as functionalized nanoparticles. The glycol capping has also enhanced the solubility of as prepared particles in aqueous medium, which further contributes the potential utilities of such particles in biological fluorescence imaging applications. The gradual variations in glycols further allow one to explore their influence on sensing ability of as synthesized Gd_2O_3 nanoparticles for p-nitrophenol (PNP) as a representative of ANCs. The changing PL emission behaviour of the functionalized colloidal Gd_2O_3 NPs with PNP has been considered as a probe in understanding the nature of aqueous-NP interface of toxin. As functionalized nano probes are potentially significant due to enhanced sensibility towards PNP with corresponding high stokes shift, better water dispersion ability and time-efficient analysis of harmful lethal ANCs in complex reaction media.

2. Experimental

2.1. Materials

All chemicals of high purity and of analytical grades were used in the experiments. Gadolinium (III) chloride hexahydrate (Sigma, 99%) was used as a precursor. Sodium hydroxide was from Merck with 99.98% purity. The ethylene glycol (EG), di-ethylene glycol (DEG), tri-ethylene glycol (TEG) and tetra-ethylene glycol (TeEG) from Fluka with 98%

purity were used as structure directing agents for Gd_2O_3 nanoparticles (Chemical structure Scheme S1 ES†). The washing solvents such as Acetone (98%) and ethanol (99.9%) were purchased from BDH and Changshu Yangyuan (China), respectively. p-Nitrophenol (PNP) with 99% purity was obtained from Sigma. HEPES buffer from Sigma was used to prepare the real sample Double distilled water was used for the solution preparations.

2.2. Synthesis of Gd_2O_3 nanoparticles

A facile synthetic process was employed to synthesize ultrasmall Gd_2O_3 nanoparticles. To describe briefly, 5 mM of $GdCl_3.6H_2O$ was mixed under stirring condition at 50 °C to 5ml of respective glycol solution in a round flask. After complete dissolution of reaction mixture, temperature of the reaction mixture was enhanced to 140°C with addition of 15 mM of NaOH pellet. The same temperature was maintained for 1 h, then enhanced to 180°C and maintained for the next 4 h. The resultant solution immediately turns out to be milky after the addition of NaOH and then, clear again with development of yellow coloured Gd_2O_3 nanoparticles. The as prepared samples were centrifuged at 4000 rpm to exclude large aggregates. The extracted particles were washed with distilled water and ethanol.

2.3. Structural characterization

The crystallite size of glycol functionalized Gd_2O_3 nanoparticles were carried out by Cu–Kα radiation (λ = 1.5418 Å) on Panalytical, D/Max-2500 x-ray Diffractometer. The optical and photoluminescence measurements were done on UV–vis. Jasco V550 and Hitachi F-7000 Photoluminescence spectrophotometer respectively. The mode of surface capping of Gd_2O_3 nanoparticles with glycols were further analysed with Perkin-Elmer (RX-1) FTIR spectrometer in the frequency range 4400–350 cm^{-1} with a resolution of 1 cm^{-1}. Nikon fluorescent optical microscope was employed to investigate the optical images of the respective samples. The surface morphology of as functionalized nanoparticles were done with Hitachi H 7500 electron microscope and JEOL (JSM-6610) scanning electron microscope (SEM) equipped with EDX analysizer at operating voltage of 100 kV and 20 KV respectively. The calcinations of the samples were done on the AICIL muffle furnace at 800°C. The fluorescence quantum yield of surface functionalized Gd_2O_3 nanoparticles were calculated by using the comparative method by employing Rhodamine 6G as reference in water (where the $\Phi_F = 0.95$).[28]

3. Results and discussion

3.1. Structure and morphological portrayal of Gd_2O_3 nanoparticles

The functionalization of exterior surface of Gd_2O_3 nanoparticles with different glycols having varied chain length has considerable impact on the dimensional characteristics of the nanoparticles. As functionalized particles have the higher water solubility which will further assist their applications in aqueous media. Figure 1 has shown the effect of glycol functionalization and influence of calcinations on the crystalline structure of Gd_2O_3 nanoparticles with the help of powder XRD analysis. The glycol coated nanoparticles does not show any characteristic peak (Fig. 1).

Fig.1.

The results were explained on the basis of amorphous nature of the particles in the presence of glycols. The variation can also been explained on the basis of interaction of glycols with the vacancy defects and the dangling bonds over the surface of nanoparticles. As a result, the corresponding Gd-O bond length is affected with glycol covering which further contributes to the variations in peak position of 2θ angle in the XRD patterns of capped nanoparticles. Moreover, the kind of microstructures and effect of particle size in the presence of different surface coverings also affect the changes in the XRD patterns. Whereas, after calcinations at 800°C, the generated particles have shown well defined peaks at 28.4°, 33.22°, 47.68°, and 56.45° comparable with the results from literature (JCPDS File No. 86-2477) (Fig. 1.). [29] No extra peak pertaining to impurities has been observed in the samples. The obtained sizes of the particles are 32.5 nm for EG, 29.3 nm for DEG, 28.1 nm for TEG and 25.3 nm for TeEG functionalized nanoparticles. The comparative role of different glycols over the agglomeration was also visualized from the TEM images of the as formed particles (Fig. S1, 2a-d). In the absence of glycols, the agglomeration tendency is more (Fig. S1), whereas in the presence of glycols, the particles are well separated with spherical morphology and fair mono-dispersity (Fig. 2a-d) with average size of 50-60 nm nanoparticles in EG, 40-50 nm in presence of DEG-coating and 35-50nm in TEG and 20-35 nm in case of TeEG-coating. It has also been visualized from the Fig. 2. that the size of the nanoparticles have inverse relationship with the chain length of the glycols. The corresponding effects were collaborated with the steric hindrance and electrostatic stabilization of the as formed Gd_2O_3 with different glycols with varied chain length. The smaller chained glycols have diffused monolayer over the surface of the nanoparticles as compared to the higher chain length glycol (Scheme 1). As a result, bigger sized nanoparticles were formed in EG capped glycol as compared to TeEG functionalized nanoparticles. Additionally, the elemental analysis of the samples has also been carried out using SEM and EDS techniques. (Fig. S2). The particles

were spherical with a certain degree of polydispersity. The higher percentage of Gd and O clearly signifies the purity of as obtained samples.

Fig. 2.

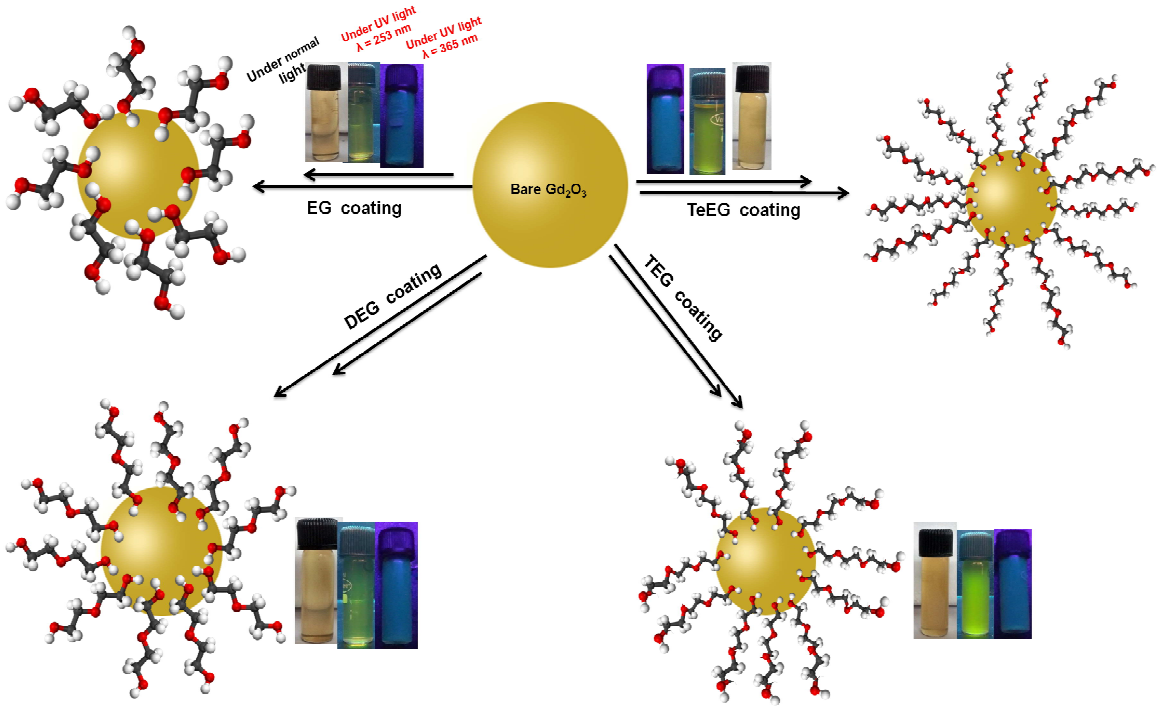

Scheme 1. Schematic illustration showing the capping of differnt glycols and digital images of Gd_2O_3 nanoparticles under normal and UV light of varied wavelength.

The generation of Gd_2O_3 nanoparticles and their stabilizing tendency in different glycols was also identified by UV-vis. analysis (Fig. S3). For all the modified Gd_2O_3 nanoparticles the spectra displayed the characteristic absorption peak in the region of 200-280 nm as compared to the peak at 300 nm for bulk nanoparticles. The presence of seven electron in 4f orbital of Gd generate around 3432 multiplets[30] with ground state corresponds to $^8S_{7/2}$ and subsequent lowest lying multiplet over ground state is $^6P_{7/2}$. Therefore the peak at 310 nm in bulk originated from the transition from $^8S_{7/2} \rightarrow {}^6P_{7/2}$.Whereas the absorption peak < 310 nm in case of surface functionalized nanoparticles corresponds to the $^8S_{7/2} \rightarrow {}^6I_{7/2}$.[31]

The surface modification also affected the peak position. In case of EG as solvent, the absorption peak has been observed at 270 nm, in DEG the absorption peak shifted to 265 nm, whereas in TEG and TeEG, absorption peak appeared at 263 nm and 240 nm respectively. The spectra of bare Gd_2O_3 have shown the absorption peak at 300 nm. These variations clearly explains the stabilizing affect of glycols with increase in chain length. From the absorption data, the optical band gap has been found be in the range of 5.3- 5.41 eV,

which was greater than the band gap of bare Gd_2O_3. Thus glycols play a vital role in shaping the morphology, size, shape and stability of the as functionalized nanoparticles. The growth of the nanoparticles is subsequently guarded by the diffused layer of the glycols over the surface of nanoparticles. Glycols afforded steric stability (due to chain length) to the as formed nanoparticles.

Fluorescence emission (PL) spectrum gave direct evidences on the nature of radiative transitions in nanoparticles as function of size, shape, morphology and nature of capping agents. The corresponding PL spectra of glycol coated Gd_2O_3 nanoparticles were shown in Fig S4 (λ_{ex} = 290 nm). The entire spectrum in each case has shown an intense broad emission peak in between 300–500 nm. This broad peak with maxima in the vicinity of 350 nm has been corresponded to $^6P_{7/2} \leftrightarrow {}^8S_{7/2}$ of Gd (III).[32] Additionally the nature of the surface covering also influenced the surface defects in Gd_2O_3 nanoparticles which further affect the asymmetry in the PL spectra for surface capped Gd_2O_3 nanoparticles. Moreover higher PL intensities in each case pointed towards the minor loss of photo generated carriers via nonradiative recombination. The electronic transformations become more complimentary for radiative recombination and hence change the fluorescence intensities in different glycols. In this manner, these surface coating further altering the photocatalytic activity of Gd_2O_3 nanoparticles.

To access the nature of the transitions, quantity of defect formation, asymmetry factor was further assessed by deconvolution of PL spectra for each system (Fig. S5). It has been speculated that in each case broad peak was split up into two peaks. The first peak corresponded to band to band ($^6P_{7/2} \leftrightarrow {}^8S_{7/2}$) and second peak was associated to the defect emissions in Gd_2O_3 nanoparticles. The corresponding asymmetry factor was calculated from the full width at half maxima (FWHM) around the main peak.[32] On interpretation, it has been found that the FWHM values varied as the function of surface capping. The increased FWHM value further corresponds to the enhancement of defect related emission as compared to band-to-band emission in Gd_2O_3 nanoparticles. The presence of different glycols influenced the densities of vacant vacancies on nanoparticles which further contribute to the defect related emission in Gd_2O_3 nanoparticles. The fluorescence quantum yield of surface functionalized Gd_2O_3 nanoparticles were calculated by using the comparative method by employing Rhodamine 6G as reference in water (where the Φ_F = 0.95). The corresponding value of Φ_F for bare Gd_2O_3 nanoparticles was found be 0.155 which is less as compared to pure dye. Moreover, the aggregation tendency of bare nanoparticles was more which further contributed towards the low Φ_F for bare Gd_2O_3 nanoparticles. The influence of surface

coverage by glycol molecules were also assessed in term of Φ_F. As compared to bare nanoparticles, the glycol coated nanoparticles have higher Φ_F values. The obtained Φ_F values of the particles are 0.23 for EG, 0.38 for DEG, 0.31 for TEG and 0.20 for TeEG functionalized nanoparticles. The surface passivation, enhanced stability and lower aggregation tendency of nanoparticles in presence of glycol molecules contributed to higher Φ_F values as compared to bare nanoparticles. The surface damage was minimised by these glycols via binding to the surface sites of Gd_2O_3 nanoparticles. The distinctive differences of Φ_F values among different glycols were based on the modulation of sizes of nanoparticles with these glycols to different extent. Moreover, with increase in the chain length of glycol i.e. for TEG and TeEG, Φ_F values had shown decrease as compared to DEG and EG. The variation is explained on the basis of the low mobility of the delocalized free electron near the conduction band of Gd_2O_3 due to the enhanced viscosity of TEG and TeEG as compared to lower chained glycols. The corresponding changes affect the vacancies of oxygen over the surface with increasing chain length of glycol and affect the quantum yield of the nanoparticles.

The variation in the peak position has also been affected in presence of glycol functionalization over Gd_2O_3 NPs. The emission wavelength has significantly red shift as a function of glycols. These behavioural variations were associated with the improvement in the emission process via defect state which was further modulated by the size of the nanoparticles. In case of EG, the emission onset shifted to the lower wavelength. This change can be explained on the basis of more nucleation in EG as compared to other glycol. The changes are also due to band gap changes with the size of particle and viscosity of the media. With increase in the chain length of glycol, the intensity of Gd_2O_3 NPs decreases due to the enhanced viscosity. The behaviour is explained on the basis of the low mobility of the delocalized free electron near the conduction band of Gd_2O_3. The corresponding changes affect the vacancies of oxygen over the surface with increasing chain length of glycol and affect the photoluminescence properties of Gd_2O_3. The corresponding changes were also analysed by illuminating the samples under UV light at λ = 253 and 365 nm (Scheme 1).

The surface modulation of nanoparticles and concentration of Gd_2O_3 nanoparticles were further correlated with the FTIR and TGA analysis. Figure S5 displayed the FTIR spectra of modified Gd_2O_3 nanoparticles. The characteristic peaks below 900 cm^{-1} are designated to Gd-O stretching vibrations for both modified and bare Gd_2O_3 nanoparticles. The corresponding C-H stretching has been obtained at 2870.72 cm^{-1}, C-O stretching peak at 1049.31 cm^{-1} and 3315.85 cm^{-1} is due to O-H stretching respectively in Gd_2O_3 nanoparticles

modified with different chain length of glycols. The peak between 1350-1480 cm^{-1} shown the bending peaks of C-H group. The lateral chain-chain interactions of glycols and their corresponding gauche/trans conformations are visualized from region between 2700 and 2900 cm^{-1} for asymmetric (ν_{as}) and symmetric (ν_s) stretching vibrations of methlyene group of different glycols. In case of EG the weak peaks are observed at 2937 and 2870 cm^{-1}, for DEG modified Gd_2O_3 nanoparticles the peaks appeared at around 2924.43 and 2857.4 cm^{-1},on the other hand TEG and TeEG modified particles displayed peaks at 2864.5, 2930 and 2864 and 2944 cm^{-1} respectively. The corresponding changes were correlated with the mode of attachment of glycol chains over the exterior façade of nanoparticles. The results were further verified with TGA analysis. Figure 3 depicts the TGA and corresponding DTA curves for glycol modified Gd_2O_3 nanoparticles.

Fig. 3.

From the graph it has been visualized that the weight loss occurred in step wise manner with 42% loss in EG-coated followed by 51.6% loss in DEG coated particles. Whereas, TEG and TeEG coated particles have shown the respective loss of ~53% and 55%. The corresponding initial step of weight losses was collaborated with the loss of moisture in the respective samples over the temperature range of 200°C. The other two consecutive weight losses occurred between 200 to 600°C. These losses were associated with the amputation of glycols templates from the exterior surface of Gd_2O_3 nanoparticles.

3.2. Fluorescence sensing of p-Nitrophenol using surface functionalized Gd_2O_3 nanoparticles

The higher sensitivity of PL emission of Gd_2O_3 nanoparticles due to the presence of surface defect was chosen as an effective tool for sensing the presence of ANCs in the reaction media. p-Nitro phenol was chosen as a representative of aromatic nitro compounds (ANCs). In brief 2ml of 5 mM Gd_2O_3 nanoparticles functionalized with different chain lengths of glycols was mixed with the different concentration (25 to 400 µl) of PNP (Fig. 4). The spectra were taken after 5 min of the reaction. Form the Figure 4, it was found that the fluorescence intensity of all the surface functionalized Gd_2O_3 nanoparticles have shown significant decrease in presence of PNP. EG modulated particles have shown higher PL intensity as compared to other surface functionalized glycols. This variation is mainly associated with the nature of the chain length of the glycols.

Fig. 4.

In presence of EG, the nucleation rate of Gd_2O_3 nanoparticles was more as compared with other surface capping as result higher PL intensities were observed in case of EG capping. Whereas, with increase in the chain length of glycols, the corresponding PL intensities of Gd_2O_3 nanoparticles have shown significant decrease of 43% for DEG, 51.95% in TEG and 15.83% for TeEG functionalized Gd_2O_3 nanoparticles in comparison with the EG functionalized nanoparticles. The variations were associated with the decrease in the mobility of delocalized free electron near the conduction band of Gd_2O_3 for higher chained glycols due to the enhanced viscosity of the media. In presence of different concentration of PNP, the PL intensities were further decreased for all the surface functionalized Gd_2O_3 nanoparticles. The fluorescence turned off efficiency was associated with the strong intermolecular interaction of PNP with the surface functionalized Gd_2O_3 nanoparticles. The interactions among the two further trap the excited electron of semiconducting Gd_2O_3 nanoparticles via electron transfer mechanism. The presence of hydroxyl group provided by the different glycols over the surface of nanoparticles further enhances the interaction of PNP over the surface of nanoparticles. The additional electrostatic and π electron cloud in PNP also augmented the interaction over the surface of nanoparticles and produced a turned off sensor with higher detection limit (Scheme 2).

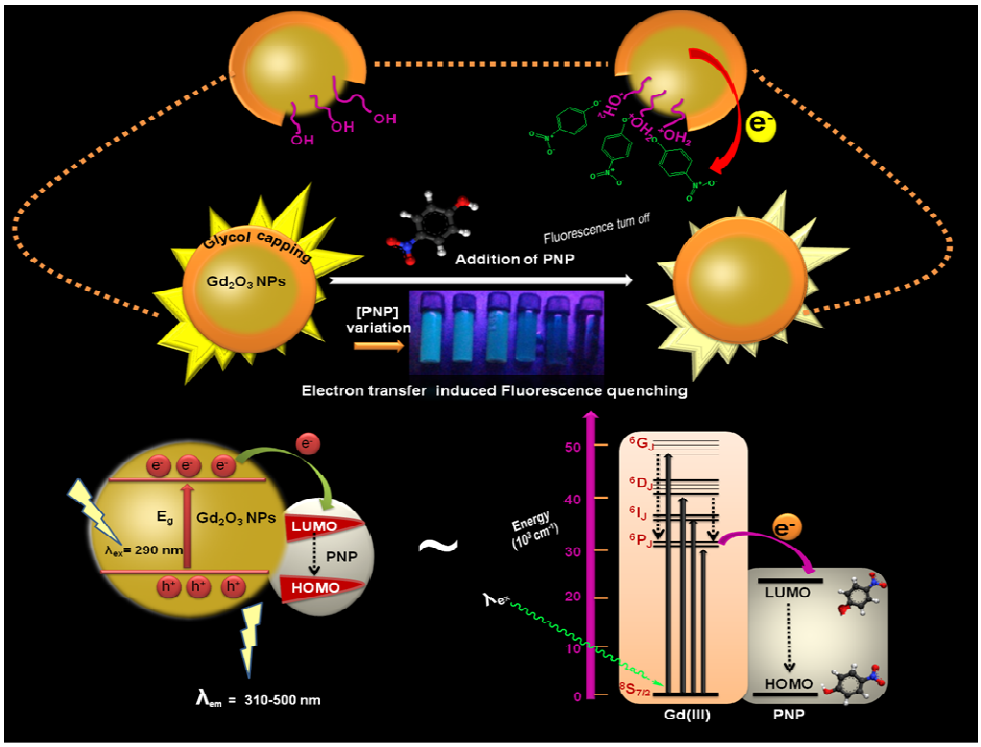

Scheme 2. Schematic illustration and mechanistic view of quenching behaviour of fluorescence intensity of Gd_2O_3 nanoparticles in presence of PNP.

In case of EG functionalized particles, the 39.1% quenching was observed upto 125µl of PNP. With further increase in the concentration of PNP in EG functionalized nanoparticles, there was significant decrease of 95.7% in PL intensity of Gd_2O_3 nanoparticles for 400µl of PNP. This variation suggested that the sensitivity of the EG modulated Gd_2O_3 nanoparticles was very high. Whereas, for DEG, TEG and TEeG functionalized nanoparticles have shown the fluorescence intensity changes for 400 µl of PNP with corresponding quenching of 88% for DEG, 39% for TEG and 44.1% for TEeG capped nanoparticles. The variation in the quenching was associated with the nature of capping over the surface of nanoparticles. The presence of different glycols influenced the mobility of delocalized electron close to the conduction band of nanoparticles and influenced the electron transfer process between the nanoparticles and PNP (Scheme 2). The intensity of the sample was further verified under UV light as a function of concentration as well as the nature of the capping over the surface of nanoparticles. The corresponding fluorescence optical microscope imaging also verified the fluorescence turn off behaviour of the surface modulated Gd_2O_3 nanoparticles towards PNP (Figure S6). The plot of F/Fo vs. log[PNP] was also drawn to assess the nature of the quenching process of surface modulated Gd_2O_3 nanoparticles against PNP. Figure 5 illustrated the linear changes for all the modulated particles. Consequently, the calibration curves were drawn for different linear concentration ranges by using modified Stern-Volmer equations.[33, 34] The spectra revels good regression coefficients with value equivalent to 0.9996 with linear range of 10-400µl of PNP. The obtained K_{SV} values for all the modified Gd_2O_3 nanoparticles were tabulated in Table S1. The corresponding detection limits were also estimated by using 3σ IUPAC criteria (Table S1). The subsequent variations in the results were collaborated with the nature of the surface binding of PNP over the surface of glycol modulated Gd_2O_3 nanoparticles. The results were also compared with available literature for PNP sensing. For instance, Pt/Poly(3,4-ethylenedioxythiophene) (PEDOT)/Prussian blue/polyazulene system was used by Lupua et al.[35]for sensing ANCs. The as fabricated sensor has shown the sensitivity of around 0.116 µA/µmol L^{-1} and LOD values of 8.23 µmol L^{-1} with regression value of 0.99108. In another report, Paliwal et al.[36] have used fluorescence-based sensing of p-nitrophenol and p-nitrophenyl substituent organophosphates by using Coumarin derivative. Yang et al.[37] have used BSA Au nanoclusters for detecting PNP using fluorescence technique. The obtained sensor have shown the linearity range of around 10^{-9} –5 × 10−5 M for PNP. Though some of the report have shown higher detection limit, but they possess lower selectivity. Whereas, the preparation process for all these modified systems were very complex and costly. On the

other hand, glycol modified Gd_2O_3 nanoparticles exhibited higher sensitivity and lower detection limit for PNP. The comparative role of different chain length of the glycols further augmented the importance of as fabricated Gd_2O_3 based fluorescence sensor for PNP. The better functionalization over Gd_2O_3 offered an efficient electron transfer mechanism and resulted in the formation of highly selective and sensitive PNP sensor. The prepared sensor has unlocked the new horizons of developments in material science for sensing harmful pollutants. The surface modulation of Gd_2O_3 have also make the sensor water dispersible and make it useful to analysis the water pollutant from different sources.

Fig. 5.

The selectivity of the system was also assessed against different ANCs and hence established that under the similar conditions. The addition of other analytes has also shown variations in the fluorescence intensity under similar reaction conditions (Figure 6.) Whereas, the fluorescence intensity was not fully quenched with these analytes as compare to PNP due to the weak binding or interaction of these analytes with surface functionalized Gd_2O_3 nanoparticles under the similar conditions and thus shown non-selective quenching of fluorescence intensity. However, despite such weak interactions, no shift of the fluorescence signal is evident in any case indicating that the sensing system for the PNP is highly tuned, functional, and selective with surface functionalized Gd_2O_3 nanoparticles. The results were verified by the strong intermolecular electrostatic interaction of PNP as compared to other ANCs with the surface functionalized Gd_2O_3 nanoparticles. These interactions among the two further affect entrapment of the excited electron of semiconducting Gd_2O_3 nanoparticles via electron transfer mechanism.

Fig. 6.

The reproducibility of the work was also examined for all the under studied systems and was found that prepared samples were quite stable with relative standard deviation of 1.1% for Eg, 1.25% DEG, 1.6% TEG and 1.4% TeEG respectively. The practical utility of the developed fluorescence sensor towards real samples were also investigated. PNP spiked measurements were performed in three different sources of water i.e. tap water, drinking water and buffer solution. The corresponding fluorescence studies for EG and DEG samples were illustrated in Fig.S7. All the samples have shown similar quenching behaviour with that of samples done in laboratory conditions. Similar results were obtained for TEG and TeEG coated nanoparticles. The average recovery and subsequent standard deviations at different spiking levels for the estimation of PNP in various samples with different glycol modulated

Gd_2O_3 nanoparticles were tabulated in Fig. 7 and Table S2. All the samples have shown the average recovering of PNP in the range of 89-97% with RSDs below 5% in most of the cases. Therefore, the current method is very selective and applicable to analysis the PNP compounds in environmental samples.

Fig. 7.

Conclusions

To summarize, Gd_2O_3 nanoparticles have been systematically synthesized using different glycols with varied chain lengths ranging from ethylene glycol to tetra ethylene glycol. The surface coating has a significant influence on the water solubility, size and emission properties of Gd_2O_3 nanoparticles. The subsequent variations in glycols further allow us to explore their influence on sensing ability of as synthesized Gd_2O_3 nanoparticles for p-nitrophenol (PNP) as a representative of ANCs. The changing PL emission behaviour of the functionalized colloidal Gd_2O_3 NPs with PNP has been considered as a probe in understanding the nature of aqueous-NP interface of toxin. The current method has also been considered as independent from the coexistence of other nitroaromatic compounds. An LOD of 3.9 x 10^{-7} M to 7.1 x 10^{-7} M was found for the determination of PNP for different surface covering of Gd_2O_3. The current process is easy, quick, economical and non-hazardous to determine PNP. Moreover, the applicability of current method towards real samples open a new pathway for detecting PNP compounds in environmental samples with higher selectivity and sensitivity.

Acknowledgement

Savita Chaudhary is grateful to DST Inspire Faculty award [IFA-CH-17] and UGC Start up Grant with reference number 20-1/2011(BSR) for financial assistance. Sandeep Kumar is grateful to CSIR India for providing junior research fellowship.

Notes and references

1. P. Eskandari, F. Kazemi and Z. Zanda, *J. Photochem. Photobio. A: Chem.,* 2014, **274**, 7–12.
2. H. Chen, L. Zhou, M. Wen, Q. Wu and C. Wang, *Mat. Res. Bull.,* 2014, **60,** 322–327.
3. C. X. Yuan, Y. R. Fan, T. Zhang, H. X. Guo, J. X. Zhang, Y. L. Wang, D. L. Shan and X. Q. Lu, *Biosens. Bioelectron*., 2014, **58**, 85–91.
4. L. Gustavsson and M. Engwall, *Waste Manage.*, 2012, **32**, 104–109.
5. M. Kulkarni and A. Chaudhari, *J. Env. Manage.,* 2007, **85**, 496–512.
6. C. C. Wang, J. R. Li, X. L. Lv, Y. Q. Zhang and G. Guo, *Energy Environ. Sci.*, 2014, **7**, 2831-2867.

7. P. Kovacic and R. Somanathan, *Med. Chem. Commun.*, 2011, **2**, 106-112.
8. P. C. Nair and M. E. Sobhia, *J. Mol. Graph. Model.* 2008, **26,** 916–934.
9. C. Hutzler, A. Luchc and J. G. Filser, *Anal. Chim. Acta,* 2011*,* **702**, 218–224.
10. T. Wellner, L. Luersen, K. H. Schaller, J. Angerer, H. Drexler and G. Korinth, *Food Chem. Toxicol.,* 2008, **46**, 1960–1968.
11. M. Mondal and A. K. H. Hirsch, *Chem. Soc. Rev.*, 2015, **44**, 2455-2488
12. A. G. Gaikwad and A. M. Rajput, *J. Rare Earths,* 2010, **28**, 1-6.
13. Y. Liu, Z. Chen, C. Liu, D. Yu, Z. Lu and N. Zu, *Biomater.,*2011, **32**, 5167-5176.
14. G. Wang, Q. Mu, T. Chen and Y. Wang, *J. Alloy Comp.* 2010, **493**, 202-207.
15. D. Niu, X. Luo, Y. Li, X. Liu, X. Wang and J. Shi, *ACS Appl. Mater. Interfaces*, 2013, **5,** 9942–9948.
16. L. Zeng, W. Ren, L. Xiang, J. Zheng, B. Chen and A. Wu, *Nanoscale,* 2013, **5,** 2107–2113.
17. T. T. N. Nguyen, V. Ruaux, L. Massin, C. Lorentz, P. Afanasiev, F. Maugé, V. Bellière-Baca, P. Rey and J. M. M. Millet, *App. Catalysis B: Env.,* 2015, **166–167**, 432-444.
18. Y. M. Zhang, Y. T. Lin, J. L. Chen, J. Zhang, Z. Q. Zhu and Q. J. Liu, *Sen. Actuators B* 2014, **190**, 171-176.
19. Y. Zhang, W. Wei, G. K. Das and T. T. Y. Tan, *J. Photochem. Photobio. C.,* 2014, **20**, 71-96.
20. G. Ferrauto, D. D. Castelli, E. D. Gregorio, S. Langereis, D. Burdinski, H. Grüll, E. Terreno and S. Aime, *J. Am. Chem. Soc*., 2014, **136**, 638-641.
21. J. Shen, L. Zhao and G. Han, *Adv. Drug Delivery Rev.,* 2013, **65**, 744-755.
22. A. Choubey, S. Som, M. Biswas and S. K. Sharma, *J. Rare Earths,* 2012, **29**, 345-348.
23. B. Elsadek and F. Kratz, *J. Cont. Rel.,* 2012, **157**, 4-28.
24. M. De, S. S. Chou, H. M. Joshi and V. P. Dravid, *Adv. Drug Delivery Rev.,* 2011, **63**, 1282-1299.
25. G. K. Kouassi and J. Irudayaraj, *J. Nanobiotech.,* 2006, **4:8,** 1-10.
26. W. H. Suh, K. S. Suslick, G. D. Stucky and Y. H. Suh, *Prog. Neurobiol.,* 2009, **87**, 133-170.
27. M. Ghiasi and A. Malekzadeh, *Superlattice Microstruct.,* 2015, **77,** 295-304.
28. D. Magde, R. Wong and P. G. Seybold, Photochem. Photobio., 2002, **75**, 327–334.
29. A. M. P. Hussain, A. Kumar, D. Saikia, F. Singh and D. K. Avasthi, *Nuclear Inst. Methods: B.,* 2005, **240**, 871-880.

30. J.G. Bunzli, S. Combay, A. Chauvin, C. D. B. Vandevyver, *J. Rare Earths*, 2007, **25**, 257-274.
31. S. Mukherjee, P. Dasgupta, P. K. Jana, J. Phys. D Appl. Phys. 2008, **41**, 215004.
32. D. L. Rogow, C. H. Swanson, A. G. Oliver, S. R. J. Oliver, *Inorg. Chem.* 2009, **48**, 1533-1541.
33. F. Friedl, N. Kraha and B. Jähne, *Sens. Actuators B.,* 2015, **206,** 336–342.
34. J. Wang, Y. Song, S. Jinyang, X. Wu, Y. Sun, X. Pan and D. Li, *Measurement,* 2013, **46**, 3982–3987.
35. S. Lupua, C. Lete, M. Marin, N. Totir and P. C. Balaure*, Electrochim.Acta* 2009, **54**, 1932–1938.
36. S. Paliwal, M. Wales, T. Good, J. Grimsley, J. Wild, A. Simonian, *Anal. Chim. Acta* 2007, **596**, 9–15.
37. X. Yang, J. Wang, D. Su, Q. Xia, F. Chai, C. Wang and F. Qu, *Dalton Trans.,* 2014, **43**, 10057-10063

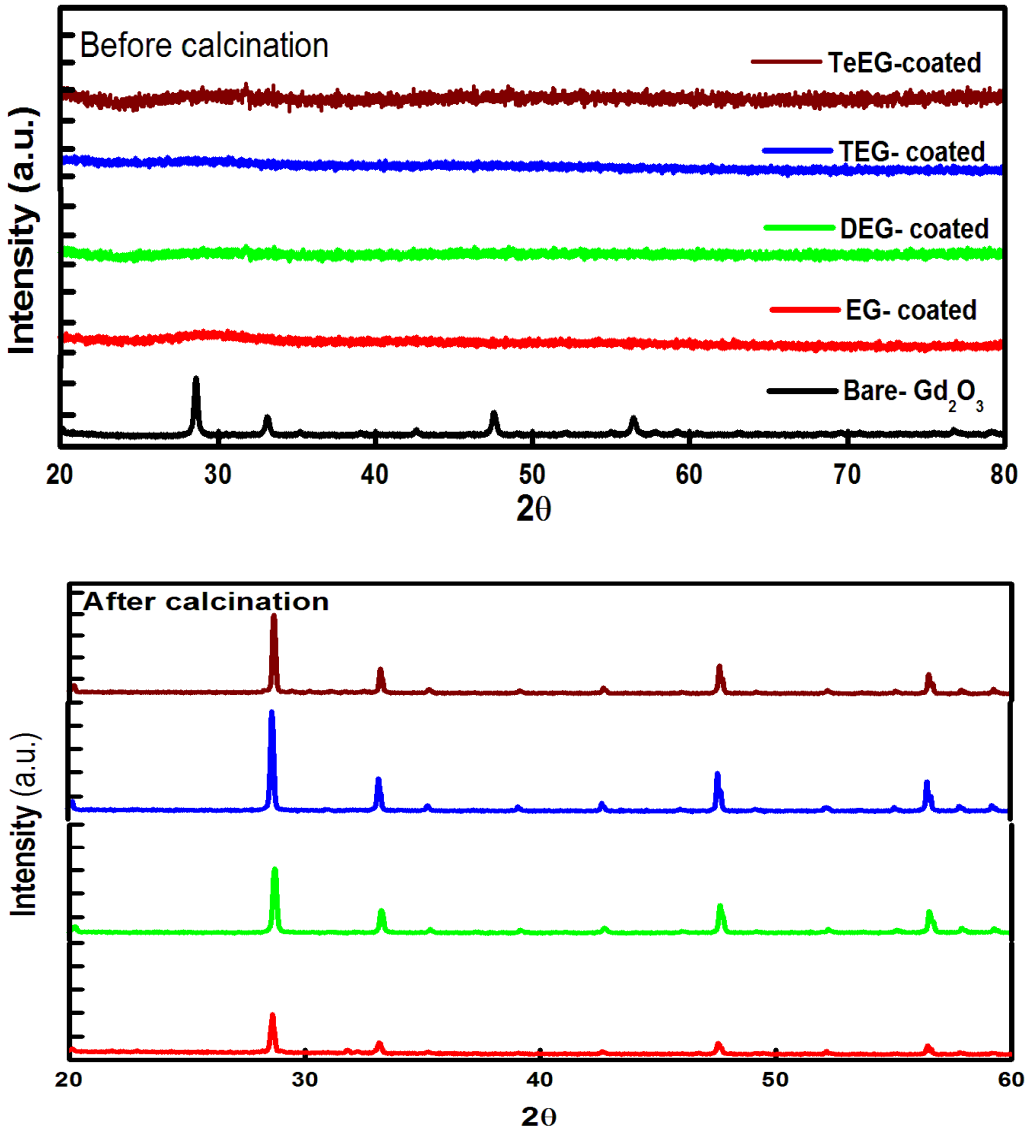

Fig.1. XRD spectra of surface coated- and calcined Gd_2O_3 nanoparticles obtained from different glycol media.

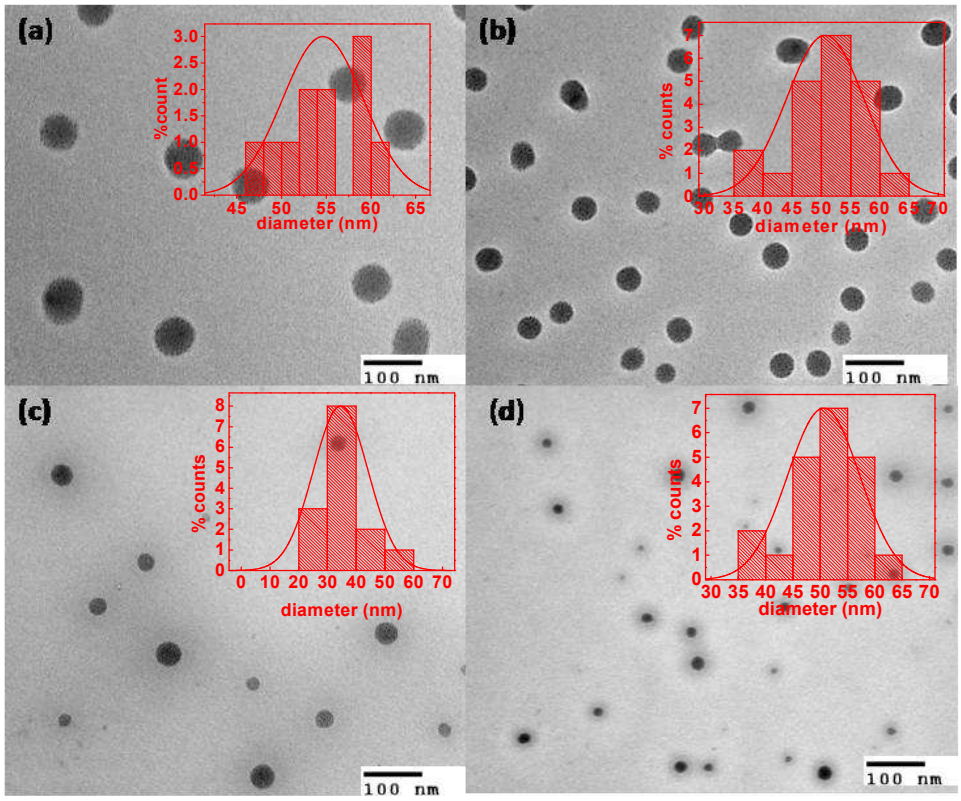

Fig. 2. TEM images of (a) EG, (b) DEG, (c) TEG, and (d) TeEG coated Gd_2O_3 nanoparticles.

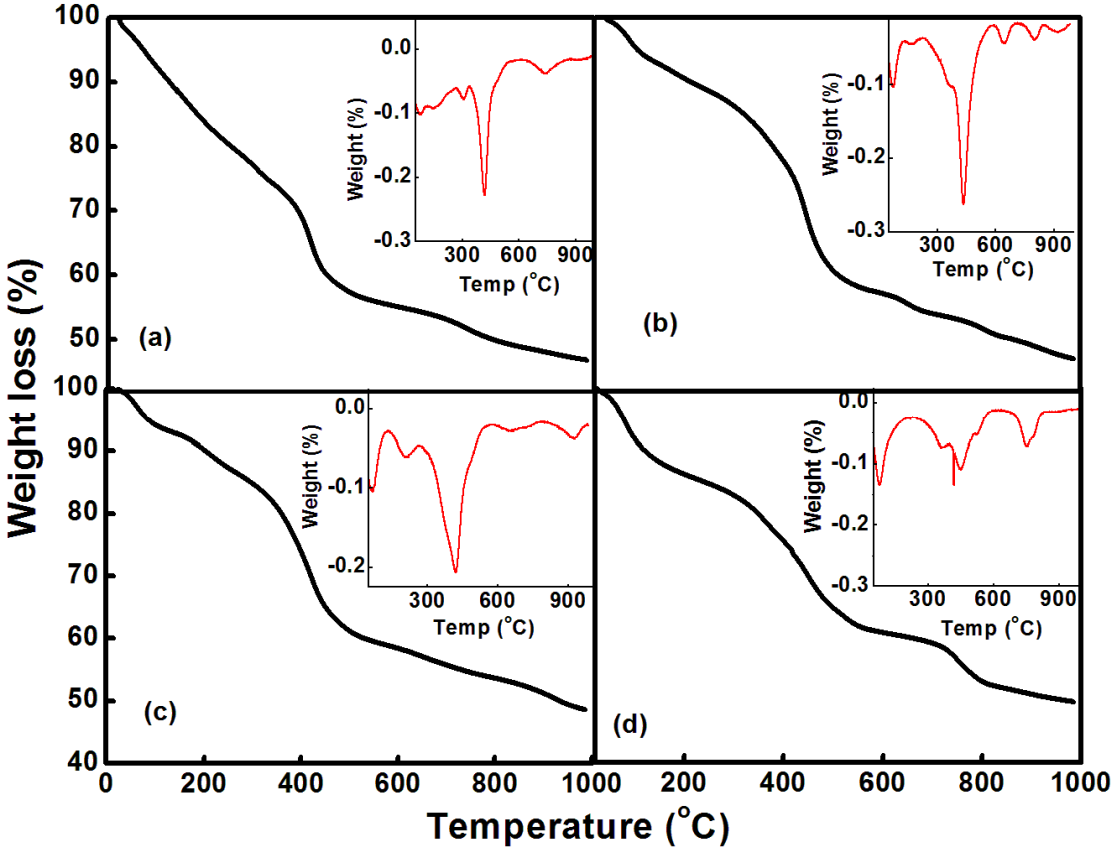

Fig. 3. TGA and DTA plots of Gd_2O_3 nanoparticles coated with (a) EG (b) DEG (C) TEG and (d) TeEG.

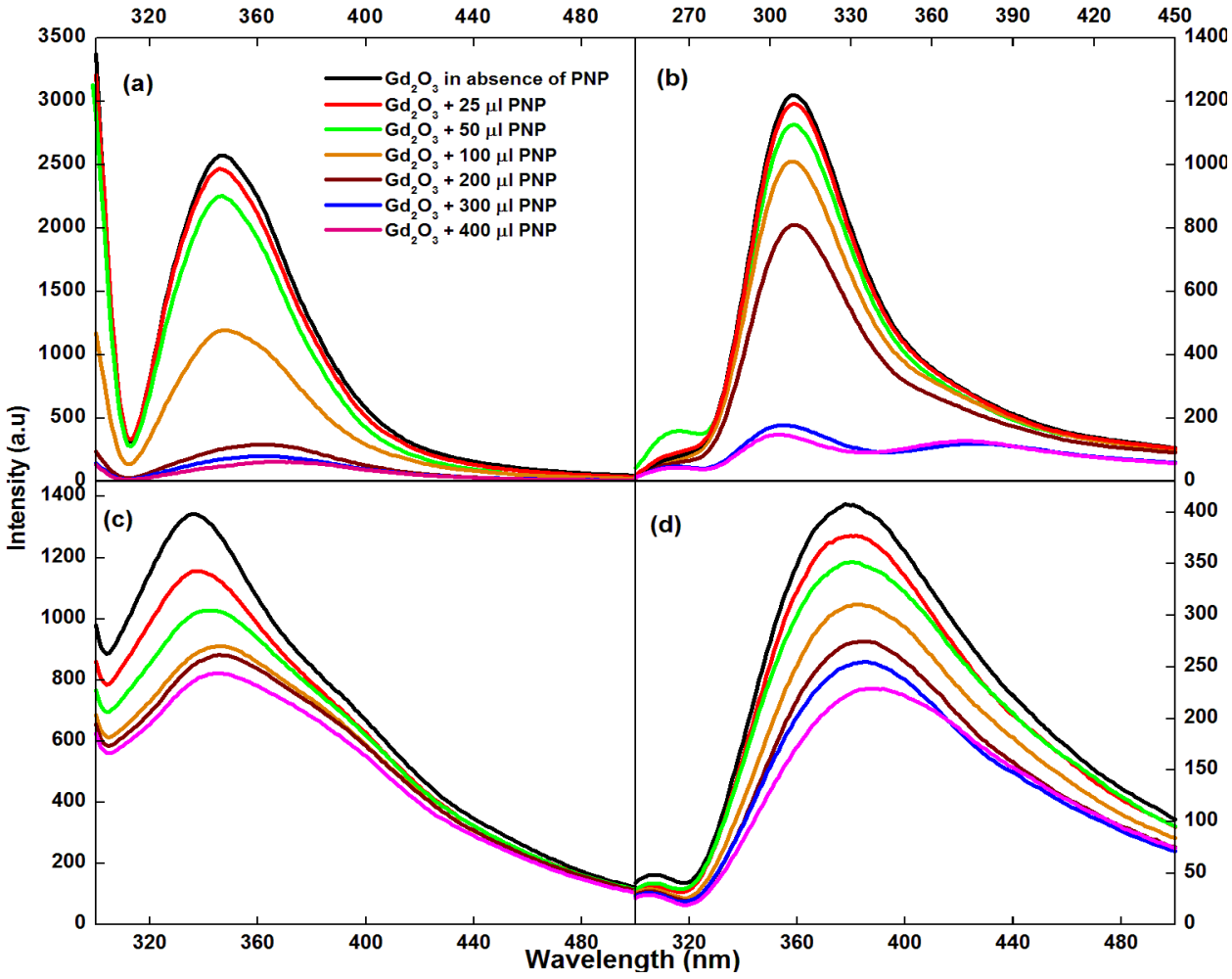

Fig. 4. Fluorescence emission spectra of Gd_2O_3 nanoparticles coated with (a) EG (b) DEG (C) TEG and (d) TeEG in presence of various concentrations of PNP.

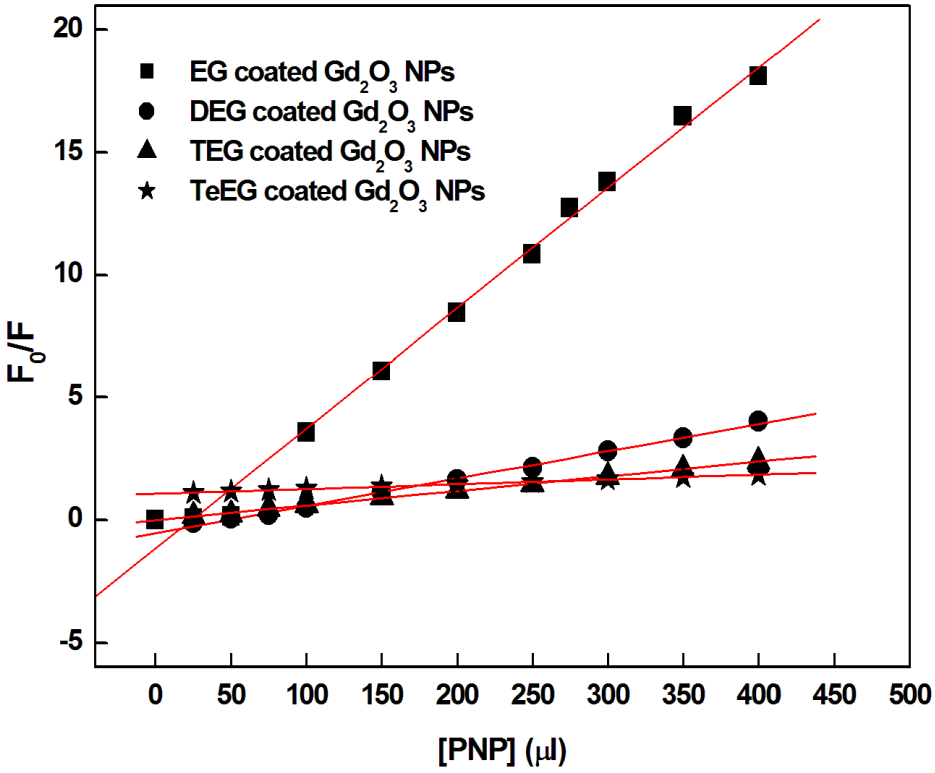

Fig. 5. Fluorescence quenching vs. concentration of PNP plot used for estimating the detection limit of PNP.

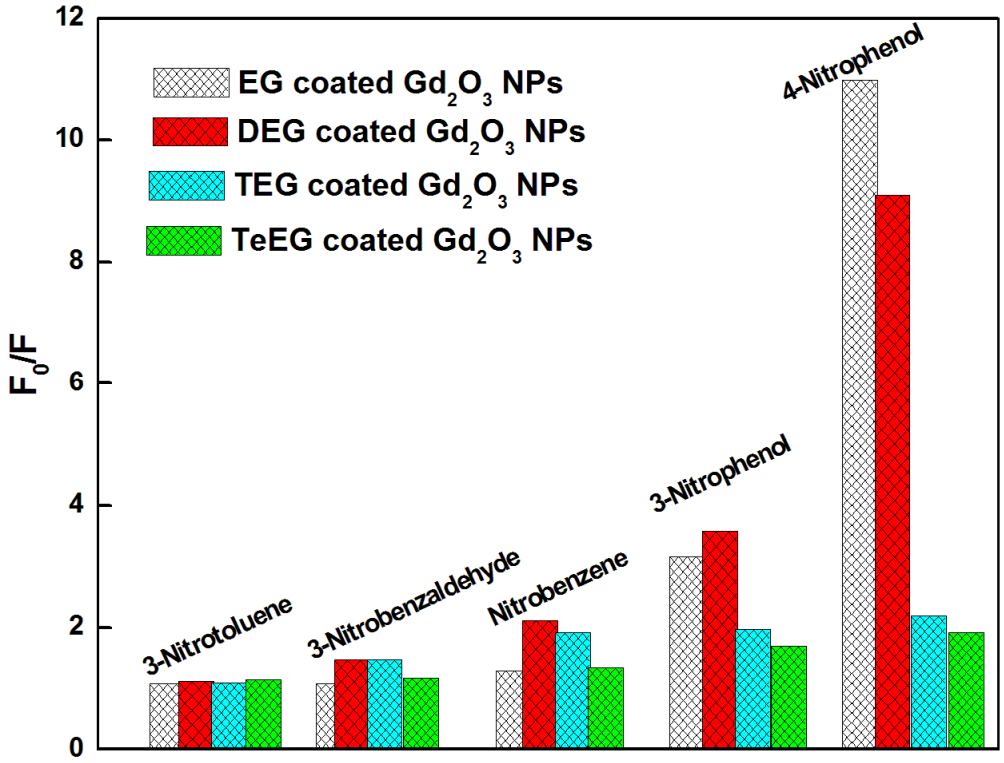

Fig. 6. Fluorescence quenching behaviour of surface functionalized Gd_2O_3 nanoparticles for different nitroaromatic compounds.

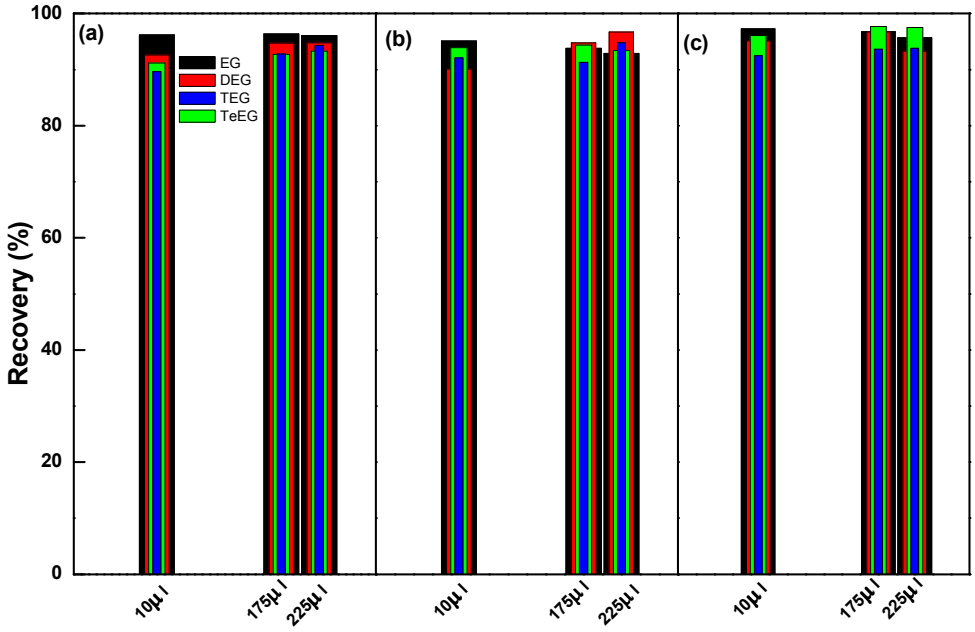

Fig. 7. The percentage recovery of PNP from (a) tap water, (b) buffer solution and (c) distilled water by using glycol modified Gd_2O_3 nanoparticles.

Graphical abstract

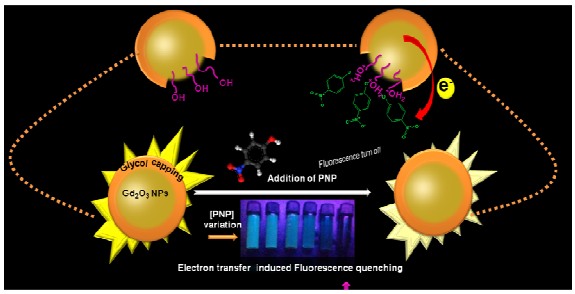

Gd_2O_3 nanoparticles based highly efficient and simplistic fluorescence sensor for PNP.